Neutron Detection Efficiency in DEAP-3600

Supervisor Aksel Hallin, Bryce Marchick 1250084[1,*]

[1]*Department of Physics, University of Alberta, Edmonton, AB, Canada T6G 2G7*

Abstract

Neutrons in DEAP-3600 can mimic WIMP signals, and a good understanding of how neutrons interact with the liquid argon scintillator and acrylic vessel is needed in order to maximize discrimination. For this study, a standalone Monte Carlo to simulate neutrons in the liquid argon and acrylic vessel was created. The detection efficiency of neutons in DEAP-3600 is good, as the monte carlo simulation of capture times (mean $490\mu s$) is only 0.4% off from the data obtained value (mean $492 \pm 22\mu s$). There is some ambiguity about Acrylic capture times, as the MC value (212 to $237\mu s$) can currently only give a range of values as the thermal energy neutrons are not well simulated. The Acrylic capture times calculated from data is $225 \pm 7\mu s$. Ar36 captures do not show up in a statistically significant way in the data. Neutrons, with an MeV energy range, that make it into the LAr must interact with the acrylic vessel due to scattering and a large mean free path at $\sim 55keV$. A prompt window of 60ns could potentially increase the WIMP exclusion by a significant factor.

*Electronic address: marchick@ualberta.ca

I. ACKNOWLEDGMENTS

I would like to thank Aksel Hallin for giving me the opportunity to work with him on this research project. I would like to give a special thanks to Shawn Westerdale for investigating the odd properties of the neutron cross section and thermalization time with me. I would also like to thank the U of A analysis team: Thomas McElroy, Courtney Mielnichuck, James Bueno and Catherine Bina. I would also like to thank Marcin Kuzniak of DEAP, and Tatsumi Koi of the CERN GEANT hadronic processess working group.

Contents

II. INTRODUCTION

One of the predictions made by the Big Bang theory, namely the amount of matter which should exist, is in contrast with observable evidence. Only 4.9% of the universe is made up of ordinary (baryonic) matter. The issue is that this unseen, or "dark matter", is not observable via EM interactions with standard particles.[1]

Fritz Zwicky, in the 1930's, first realized that there is more matter than observable via visual optics in galactic clusters. Using the orbital motion and the Virial theorem, only about 13% of the mass in a cluster is visible. The rest was what he called dunkle Materie (dark matter)[2].

One of the best candidates for dark matter is a particle that interacts gravitationally and through the weak force, the so called "weakly interacting massive particles", or WIMPs for short. The DEAP-3600 experiment, standing for "Dark matter Experiment using liquid Argon Pulse shape discrimination" is designed to detect the presence of WIMPs through scintillation of liquid argon.

III. DETECTOR THEORY

DEAP-3600 uses liquid argon (LAr) as a scintillator, that, when struck by a high energy particle, ionizes and forms an excited state. Argon generally refuses to interact with other elements or compounds, but when excited, it will form an excited dimer (also known as an excimer). Excimers rapidly de-excite to lower energies until they are either in a singlet or triplet lowest energy state [3] A higher interaction energy produces more singlet states, since recombination is faster; thus the excimers produced have less time to transition to the singlet state. LAr is also transparent to its own scintillation light.[3, 4]

When the WIMPS collide with the LAr, it recoils from momentum conservation. In LAr, nuclear recoils tend to excite to the singlet state and sometimes the triplet, while electromagnetic (EM) interactions tend to excite into triplet states and sometimes the singlet.[3, 4] This behaviour is called Pulse Shape Discrimination (PSD).

Scintillation is the only means of detection in DEAP-3600. This results in a higher light yield when compared to double phase detectors, and thus a better discrimination between particles. [3, 4]

IV. BACKGROUND MITIGATION

DEAP-3600 was constructed using radio-pure materials, which are simply normal materials but with a low specific activity. Similarly, materials brought down to the detectors working area are cleaned and checked for radioactivity prior to being allowed into the lab. Prevention of surface contamination on the acrylic was done using a resurfacer, which removed a tiny fraction of the acrylic surface and cleaned it.

DEAP-3600 was placed deep underground to reduce cosmic background noise, but extra care is needed to account for seismic and radiological events. Other events, such as neutron, α and β, can be mitigated via physical shielding (neutrons and α) and PSD (β) as seen in Table.I.

Since the detector can not be completely isolated from background events, there needs to be further discrimination between recoils and background events. β particles produced from the decay of ^{39}Ar, and γ radiation dominate the background. These can be easily distinguished via PSD. α particles can not be distinguished via PSD, but they deposit an immense amount of energy that makes their signal obvious. Neutrons, however, mimic the WIMP signal very closely, meaning excellent shielding is needed. That said, there remains the issue of asking "what if a neutron does make it into the detector? How will we distinguish between a neutron in the WIMP ROI and the WIMP itself?".

Background	Mitigation	Events passing energy cut	Events passing energy, position and pulse shape cuts
Neutrons	Acrylic light guides, filler blocks	30	<0.2
Surface α	Material choice, resurfacing	150	<0.2
^{39} Ar β	Pulse shape discrimination	$1.6 * 10^9$	<0.2

TABLE I: Expected events for 3 years of data-taking. Data Credit: Ben Smith 25-08-15

V. NEUTRON INTERACTIONS

The governing factor in how a neutron interacts with matter is determined by the cross section. Everything from scattering, absoprtion, excitation, gamma emission, etc, is represented by a an "effective target area" which can be thought of as an associated "probability" for each type of interaction. Fig.1 shows all of the relevant cross sections.

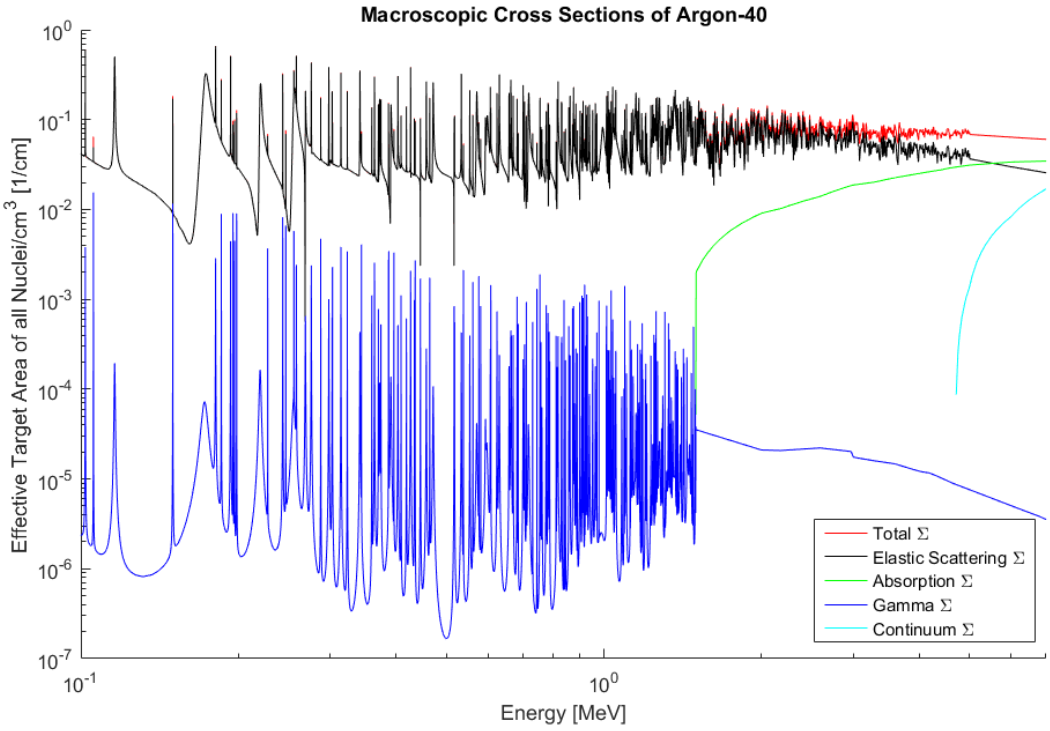

FIG.1 : Data taken from NNDC, plotted in MATLAB. Notice that continuum scattering goes to 0 for energies below 4.5 MeV, and Absorption goes to 0 below the first excited state of 1.46 MeV. Absoprtion also has a higher macroscoptic cross section than scattering above 5MeV, and is still comparable until 2 MeV.

The DEAP collaboration group uses RAT (Reactor Analysis Tool), which uses CERN's GEANT4 physics simulator to do complicated MC (Monte Carlo) simulations. Considering that the cross sections are rather complicated around the MeV range, there was concern that RAT did not have the correct cross sections. A comparison between the current library on NNDC (ENDF/B-VII.1) and the latest library version in GEANT4 (ENDF/B-VI) is shown in Fig.2.

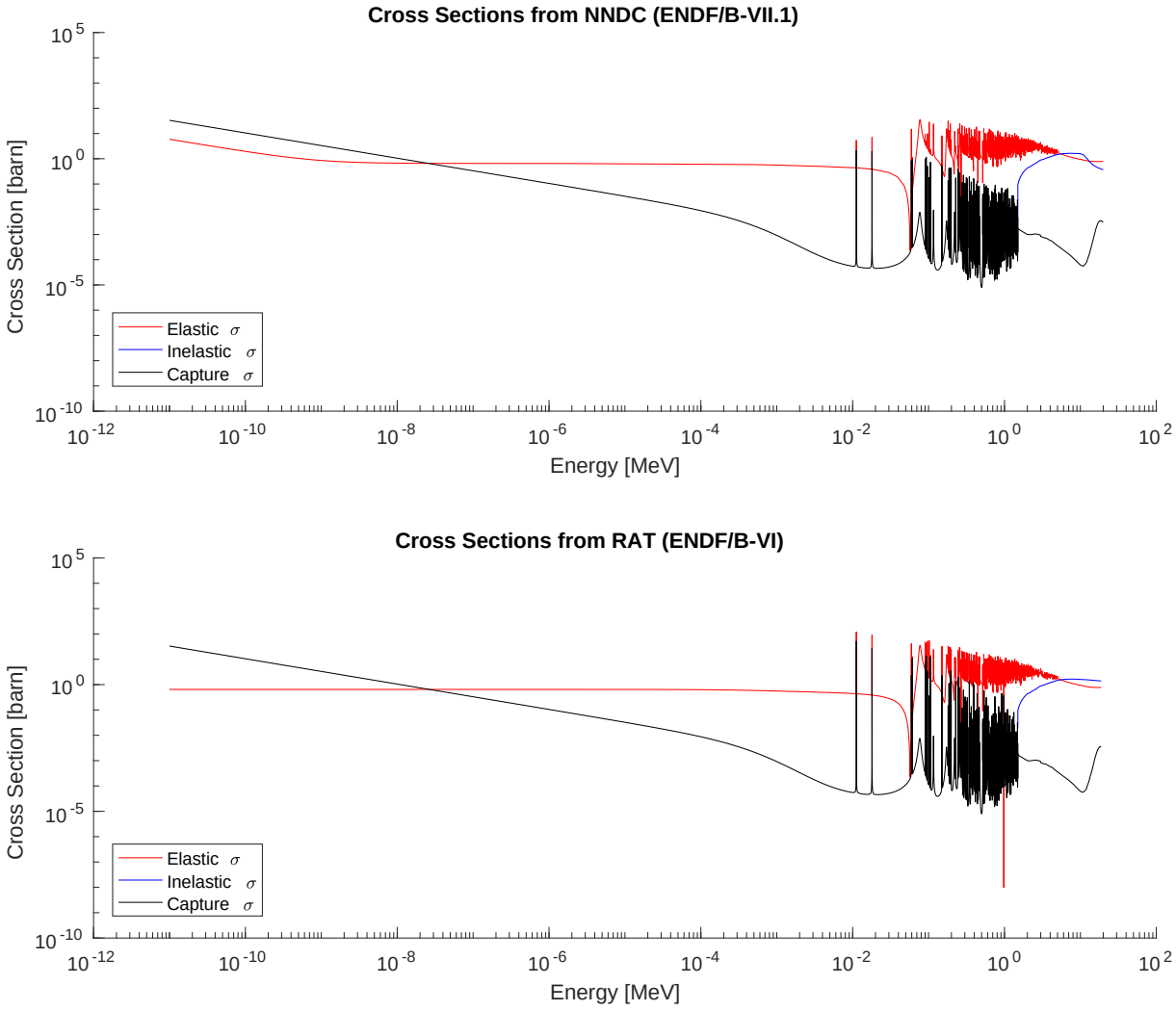

FIG.2 : Data taken from NNDC, plotted in MATLAB, compared to those found in GEANT4. Some key missing features from the RAT cross sections include the increasing

capture σ below 0.1eV, the inelastic cross section not going below the scatter above 7MeV, the scatter going down to 10^{-8} barns around 1MeV which is not present in the NNDC data, and the twin peaks around 10^{-2} MeV are incorrect in relation to each other.

Upon discussing this with Tatsumi Koi (CERN Hadronic Processes working group) and Marcin Kuzniak (DEAP), GEANT itself will be updated to the latest version as the cross sections, radioactive decays (needed for pmt neutrons via C13+/*alpha* interactions), optics, etc. are all improved. This update will occur after the first analysis is completed.

VI. NEUTRON INTERACTION THEORY

The neutron-nucleus interaction is dominated by the strong force, but the interaction of the neutron spin with unpaired electron density in the material can contribute to cross sections. In addition, other electromagnetic interactions of the neutron with the nucleus and the atomic electrons may contribute to the cross section of the scattering process, including the spinorbit and Foldy interactions, as well as those related to the electric polarizability and the finite intrinsic charge radius of the neutron [9, 10]. These secondary interactions are typically a few orders of magnitude smaller than the nuclear interaction, but can become significant for certain neutron energies. The electronic interactions can be calculated from the electronic structure of the atoms, but the strong interaction relies on the detailed structure of the atom. Therefore, the main deciding factor in scattering length has to be measured.

A. Elastic Scattering

Here, energy and momentum are conserved. The energy given to the target atom is entirely dependent on the collision angle and mass of the target atom. As elastic scatters are typically the dominant mode of interaction, it is possible to determine the average number of collisions it takes to go from an initial energy to a final energy. The kinematics of this collision can be obtained from the process described in section VII.

B. Inelastic Scattering

For an inelastic scatter, energy is lost to exciting the target atom. This energy is eventually released by a photon with a characteristic energy (1.4MeV for Ar40), and so detection of this 1.4 MeV γ can veto these neutrons. The neutron will then continue to scatter and interact with the LAr. The kinematics of this collision are derived in section VII.

C. Capture, Fission, Continuum Scattering, etc.

Processes involving radiative capture, (n,p), (n,α) and (n,2n) etc., are related to the imaginary component of the complex valued scattering length [9, 10]. There is no accurate descriptor of these processes, so they too must be measured.

As (n,γ) interactions can potentially occur at any point throughout the scattering process, the amount of detected photoelectrons by the PMTs will be proportional to the neutrons energy, and will occur at a single point. These radiative captures can occur with high probability in the resonance region. The energy of the neutron is taken to be exactly zero after this interaction occurs, and Ar40 captures to Ar41, which has a half life of $\sim$109 minutes and decays through β^- to K41 which is stable.

D. Scattering Length

Note: The following derivation is only valid for slow neutrons ($< \sim$10 eV) where the spatial range of neutron-nucleus interactions is negligle compared to the neutron wavelength. For a more complete picture, neutron-atom interactions are needed, which is nicely shown by Fernandez-Alonso and Price, along with spin-dependent scattering lengths [10], and their neutron-nucleus interaction derivation is summarized below.

1. A neutron of energy E propagates along z, interacting with a nucleus of infinite mass. This restricts the process to elastic scattering. The nuclei are also considered to be free, as is the case in LAr. This changes the bound scattering length b to the free scattering length $a = Ab/(A+1)$.

2. The wave function that solves the scattering problem is:

$$\psi(\vec{r}) = exp(ikz) + \frac{e^{ik\vec{r}}}{r} f(\vec{k}) \tag{1}$$

where the first terms is the incident wave, and the second is the scattered wave whose propagation vector is $\vec{k} = k(\vec{r}/r)$ with amplitude

$$f(\vec{k}) = -\frac{m_n}{2\pi\hbar} \int e^{-i\vec{k}\cdot\vec{r'}} U(r')\psi(\vec{r'}) d\vec{r'}. \tag{2}$$

3. For thermal neutrons, the range of nuclear forces is negligible compared to the neutron wavelength, so $\vec{k}\cdot\vec{r'} << 1$ (S-wave scatter approximation), and the scattering amplitude admits an expansion in powers of k:

$$f(k) = -a + ika^2 + O(k^2), \tag{3}$$

where a is the scattering length and is normally determined experimentally. A good approximation for thermal neutrons is $f(k) \approx -a$ as $|ka| \approx 10^{-4}$.

4. Assuming that the atom is in the ground state (nuclear and electronic) and remains in the gs after the collision, the scattering length a can be calculated with the Born approximation:

$$f(\vec{k}) = \frac{m_n}{2\pi\hbar} \int U(r) e^{-i\vec{Q}\cdot\vec{r}} d\vec{r}, \tag{4}$$

where $\vec{Q} = \vec{k_i} - \vec{k_f}$, the difference between the incident and scattered wave vectors.

5. The scattering length is complex: $a = a' - ia''$ and it's imaginary (absorption) is usually of the same order of magnitude as the second term in equation (3).

6. In cases where $f(k) = -a$ and the scattered wave is described by the first Born approximation, the Fermi pseudo-potential describes $U(r)$:

$$U(r) = \frac{2\pi\hbar^2 a}{m_n} \delta(r). \tag{5}$$

Note that this is not valid when the imaginary part of $f(k)$ is relevant.

7. The scattering amplitude of an atom is directly related to the differential cross section:

$$\frac{d\sigma}{d\Omega} = |f(\vec{k})|^2 = |a|^2(1 - 2ka'') \tag{6}$$

neglecting higher terms. For S-waves this is independent of the angle.

8. Integrating this in all directions, the scattering cross section is obtained:

$$\sigma_S = 4\pi|a|^2(1 - 2ka'') \tag{7}$$

9. The total scattering cross section is obtained from

$$\sigma_T = \frac{4\pi}{k} Im[f(\vec{k})]_{\theta=0} = \frac{4\pi}{k} a'' + 4\pi(a'^2 - a''^2) \tag{8}$$

10. As $\sigma_T = \sigma_S + \sigma_A$, the absoprtion cross section can be easily obtained:

$$\sigma_A = \frac{4\pi}{k} a''|1 - 2ka''| \tag{9}$$

As previously stated, $ka'' << a$, so $\sigma_S = 4\pi|a|^2$ is commonly used, meaning $\sigma_A = \frac{4\pi}{k}a''$. This simplification for σ_A is commonly known as the "1/v" law for absorption.

For the special case of resonance (due to internal nuclear particle arrangements), the scattering length is corrected by adding the Briet-Wigner terms:

$$b = R + \frac{\Gamma_{n,r}/2k}{E - E_r + i\Gamma_r/2} = R + b_r(E), \tag{10}$$

where R is the scattering length due to potential scattering (the direct scattering term due to the presence of an interaction potential) and $b_r(E)$ is the resonance scattering length. Here, E_r is the energy of the r-th resonance, $\Gamma_r = \Gamma_{n,r} + \Gamma_{\gamma,r}$ is its total width, and E is the incident neutron energy in the CoM frame.

VII. NEUTRON-40AR KINEMATICS

Note: The following derivation is for the inelastic cross section interaction, but elastic can be obtained simply by setting $Q = 0$. If interaction via capture occurs, then the current energy is entirely deposited into the Argon atom and no more collisions can occur.

To excite a nuclear level of the target nucleus of energy Q above the ground state, the neutron must have an energy $E \geq \frac{A+1}{A}Q$, which in the case of LAr gives $E \geq 41/40Q = \epsilon$.

In the lab frame, energy E and momentum p are conserved:

$$\vec{p} : m\vec{v} = m\vec{v'} + m_{Ar}\vec{v'}_{Ar} \tag{11}$$

$$E : \frac{1}{2}mv^2 = \frac{1}{2}mv'^2 + \frac{1}{2}m_{Ar}v'^2_{Ar} + Q, \tag{12}$$

where prime indicates after collision.

Converting to the centre of mass (CoM) frame:

$$\vec{u} = \vec{v} - \vec{v}_{CoM} = \frac{40}{41}\vec{v} \tag{13}$$

$$\vec{u}_{Ar} = -\vec{v}_{CoM} = -\frac{1}{41}\vec{v}. \tag{14}$$

Total momentum p_T and total energy E_T are conserved, so

$$\vec{p}_{T,CoM} = 0 \Rightarrow m\vec{u} + m_{Ar}\vec{u'}_{Ar} \tag{15}$$

$$E_{T,CoM} = \frac{1}{2}mu^2 + \frac{1}{2}m_{Ar}u_{Ar}^2 = \frac{1}{2}mu'^2 + \frac{1}{2}m_{Ar}v_{Ar}'^2 + Q \tag{16}$$

$$\Rightarrow u' = \frac{40}{41}v\sqrt{1 - \frac{41}{40}\frac{Q}{E}}. \tag{17}$$

For the neutron speed in the lab frame:

$$\vec{v'} = \vec{u'} + \vec{v'}_{CoM} = \vec{u'} + \frac{1}{41}\vec{c}, \tag{18}$$

$$\Rightarrow \vec{v'}^2 = \vec{u'}^2 + \frac{1}{41^2}\vec{v}^2 + \frac{2}{41}\vec{u'}\vec{v}\underbrace{\left(\frac{\vec{u'}\cdot\vec{v}}{|\vec{u'}||\vec{v}|}\right)}_{\mu_{CoM}}, \tag{19}$$

So that finally,

$$\frac{E'}{E} = \frac{\vec{v'}^2}{\vec{v}^2} = \frac{40^2(1 - \frac{41Q}{40E}) + 80\sqrt{1 - \frac{41Q}{40E}}\mu_{CoM} + 1}{41^2}. \tag{20}$$

Here, μ_{CoM} is taken to be isotropic and random at each collision. For this study, $Q = 1.46$ MeV, the first excited state of 40Ar. This also coincides with the threshold energy of the inelastic cross section shown in Fig.2.

VIII. NEUTRON SIMULATION (MONTE CARLO BASED)

First, a description of how the simulation works is provided for orientation. Each possible interaction (cross section) is treated as a separate entity. The mean free path (mfp) is

calculated for each at the interpolated neutron energy. Then, the mfp's are "jittered" around an exponential with a peak at the calculated mfp, and the lowest resulting mfp is chosen to be the interaction that occurs. This allows for an arbitrary amount of isotopes and cross sections to be easily added.

Several things were ignored for this simulation, but can be justified. Doppler broadening is very minimal when thermal is $\frac{7}{1000}eV$. Resonant lifetimes are large (due to the sharp peak), but this is on the order of $10^{-20}s$ and is insignificant for the number of collisions that occur in the resonance region (≈ 86 per neutron). Fission interactions, (n,n_c), (n,α), etc all occur at energies higher than 4MeV.

The energies of a typical "scattering only" neutron in LAr (pure Ar40) is shown below in Fig.3. We see that, when compared to the cross sections in Fig.2a, the first large dip around 10^2s occurs when the inelastic interaction occurs. The exceptionally large gap starting around 10^4s corresponds to the large dip in the scattering cross section around 55keV (not seen well in Fig.1 or 2). This indicates that once neutrons reach this energy level, they must interact with the Acrylic, filler blocks, etc as the mfp is many orders of magnitude larger than the diameter of the LAr. Therefore, a more accurate MC requires the addition of the acrylic shell and proper boundary conditions. This addition was not completed for this study, but I am working on it.

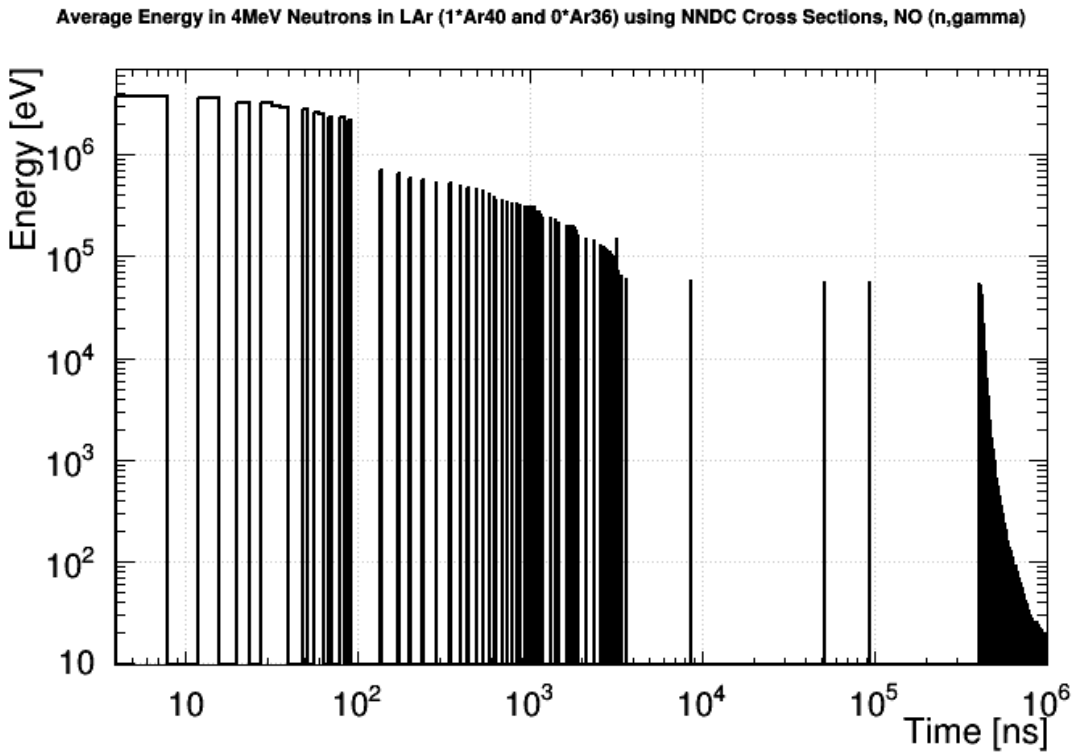

FIG.3 : Sanity check of a single neutrons energy as it scatters through the infinite pure liquid Ar40. There is no (n,gamma) interaction in this simulation.

With the newest library data, we can directly compare simulations done with the Reactor Analysis Tool (RAT) cross sections to a MC taking the latest NNDC data (see Fig.2a) into account. This will tell us if previous RAT MC simulations can be trusted. To do this, we generate tens of thousands of neutrons, and determine the amount of time it takes to capture or thermalize. Capture can happen at any point as the neutrons scatter in liquid Ar40, but the thermalization is taken to be a lower limit the neutron can have. This is also something that can be determined from DEAP-3600 data by looking at gamma followers, so direct comparisons between MC, RAT and data are possible. Below, in Fig.4, we see the capture times for simulated 4MeV neutrons in LAr.

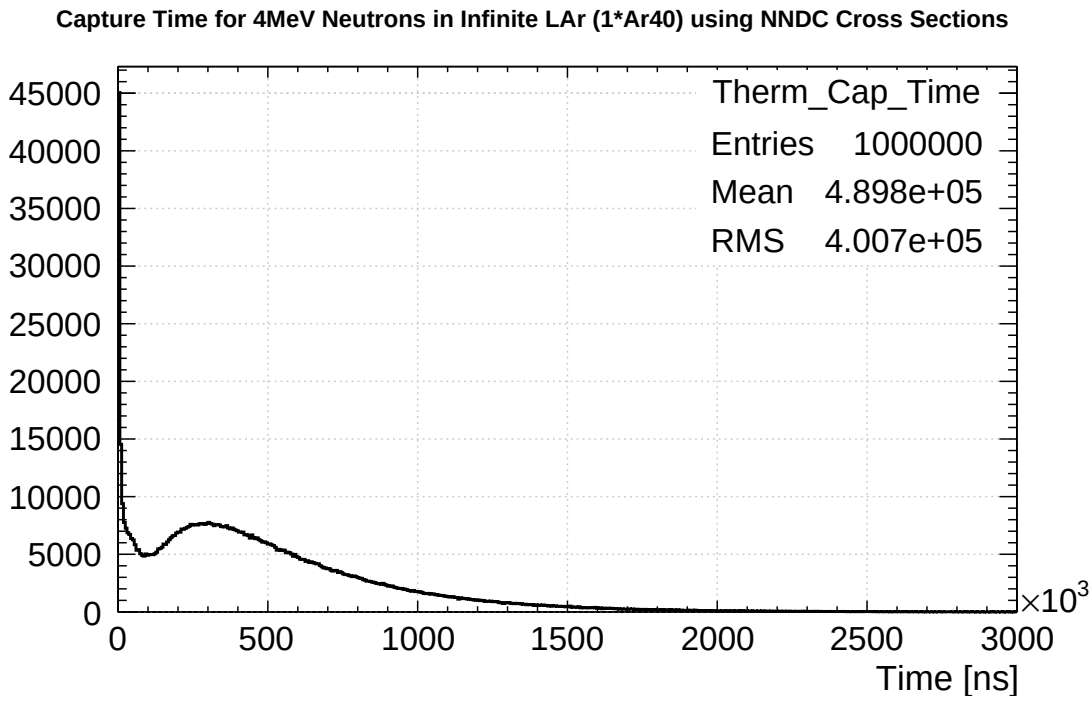

FIG.4 : Simulation of the time to capture/thermalization of 1,000,000 neutrons. Notice that there is a peak around 350μs, and a tail that pulls the mean capture time up, countered by a number of quick captures that pull the mean down.

IX. BREAKDOWN OF LAR CAPTURE TIME PROFILE

From simulation (Fig.4), we see some neutrons experience quick capture within the first few collision and a gamma ray is emitted with an energy equivalent to the appropriate level. From counting the number of captures before the end of the resonance ($\approx 1keV$), it was determined that nearly 25% of neutrons capture in the resonance zone as (n,γ) is comparable to $\sigma_{elastic}$. This should be detectable and removed automatically by fprompt cuts. The majority however, continue through elastic scattering until they are captured when the capture cross section becomes relevant as seen in Fig.2.

Once the neutrons are approximately thermal, the capture time is independent of energy because the cross section is proportional to $1/v$ [5, 6]. Shawn Westerdale has recently completed an independent study of capture times in LAr, and has reached the conclusion that "The thermal neutron capture time [...] in LAr [should be around] 343 μs" [7]. Using an initial energy of 0.007eV (thermal energy for DEAP-3600 LAr), we see that the MC

suggest a capture time of around 324 μs shown in Fig.5. Notice also, that it becomes very exponential-like. This is also what Shawn reported. Therefore, it appears that $\sigma_{inelastic}$, the resonance zone and the $55keV$ dip significantly contribute to capture times, but how much they contribute is not yet known.

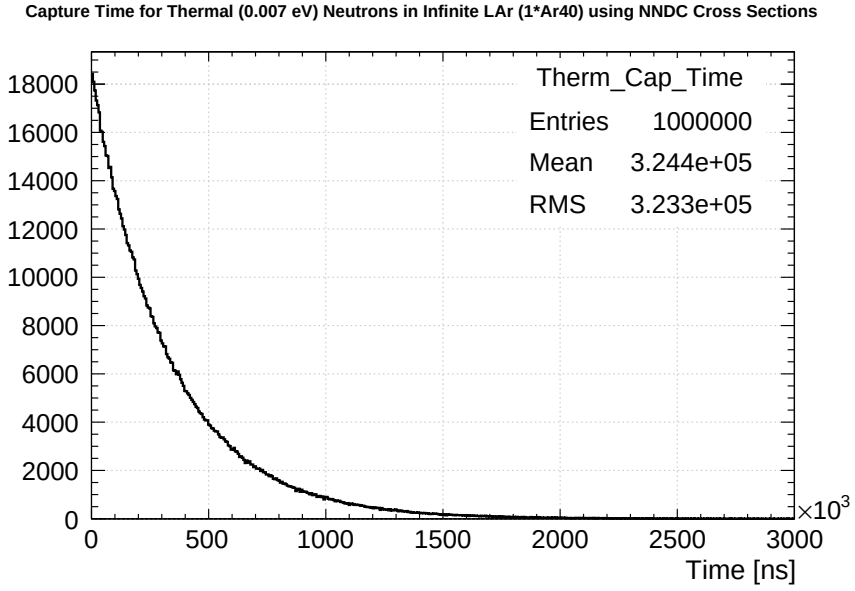

FIG.5 : Simulation of the time to capture/thermalization of 1,000,000 neutrons with an initial energy of 0.007 eV. Exponential-like decays are due to the statistical nature of capture, and that the mfp is jittered around the value extracted from NNDC.

So, the question about why the mean is stretched out and not comparable to the mode around 350 μs seen in Fig.4. If the peak is due to the neutrons that capture quickly, then the tail is possibly from neutrons that take longer to thermalize. The particular shape shown in Fig.4. can possibly be explained as the result of the convolution of two exponentials: thermalization time and capture time. Discrepancies between this MC result and Shawn's result could come from the thermalization process. He argued that "the elastic scattering cross section for argon may be higher than for hydrogen because of the nuclear size, so that should mitigate the difference some), though there could be nuclear structure differences that matter" [5], but the H1 cross section is almost 100 times larger than 40Ar at all energies below 10keV. He then suggested that thermalizations times now seem to be the main cause of his discrepancy; "Due to kinematics, neutrons need to scatter 10x more to thermalize. Looks like the cross section is about 70x higher for fast neutrons under a few tens of keV

in hydrogen than in argon. So maybe this can explain a lot of the difference" [5]. Also, he only looked at thermal neutrons, but as noted previously, cross sections above resonance contribute to capture times significantly. The $55keV$ dip also increases capture times by $\approx 100\mu s$ seen in Fig.6.

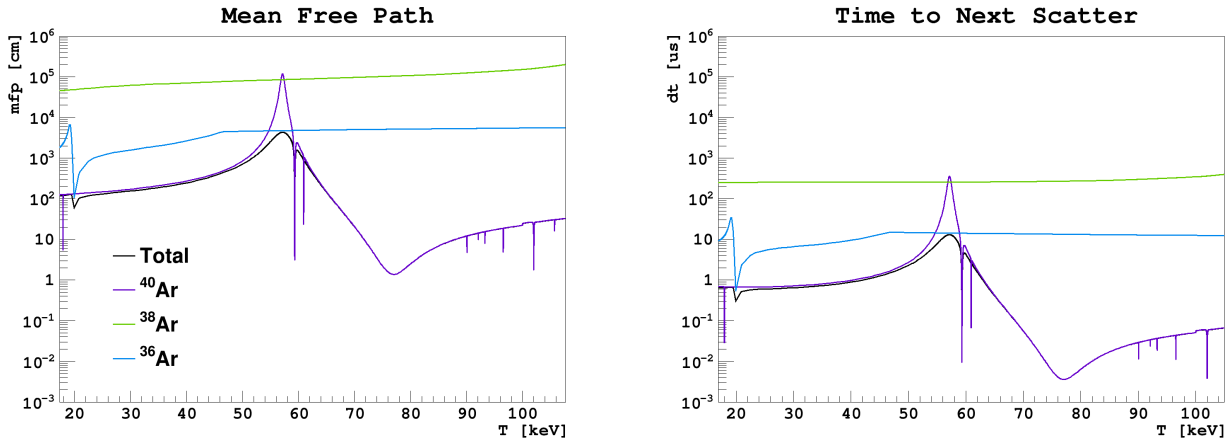

FIG.6 : Comparison of Ar40, Ar38 and Ar30 cross sections in the "abnormally high mfp region" in Ar40. Image Credit: Shawn Westerdale 09/03/17

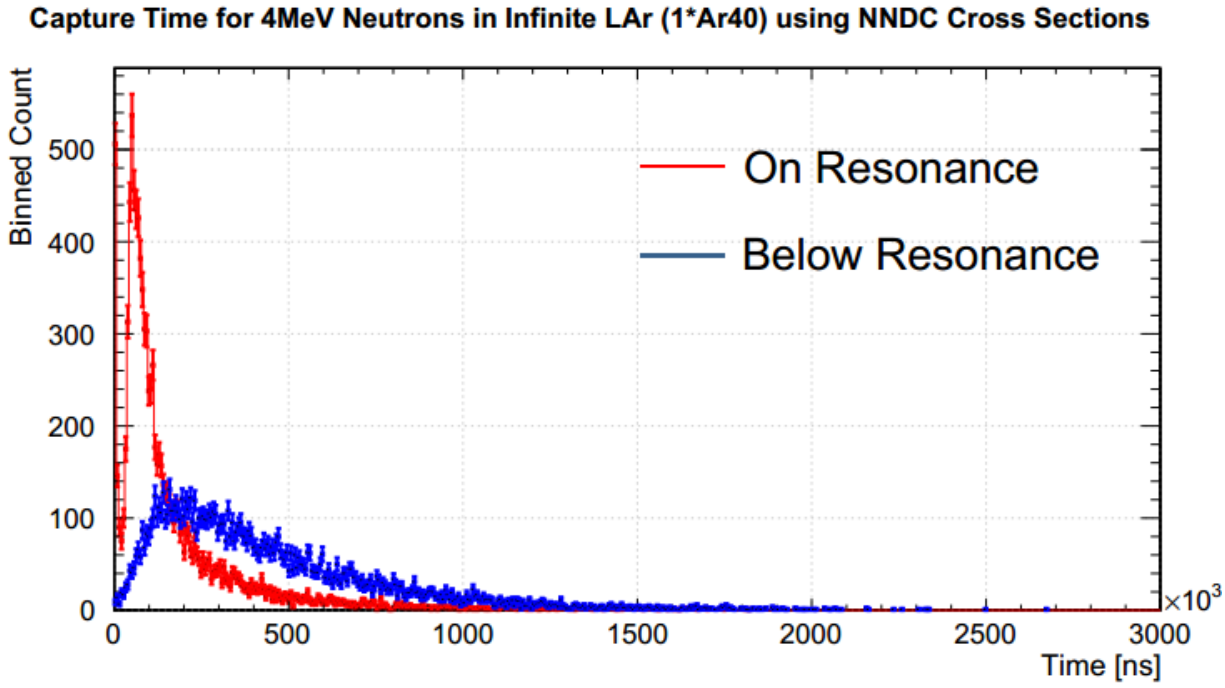

FIG.7 : Capture times simulated in two regions: the energies on resonance for Ar40, and energies below resonance for Ar40. Note that there are many quick captures on resonance, and none below resonance.

X. ACCOUNTING FOR AR36 IN LAR

This simulation, however, can account for both Ar40 and Ar36 in whatever ratio is needed (natural abundances are used for futher analysis). Shawn Westerdale speculated that due to Ar36's much higher cross sections (around 100x higher) that it would have a significant effect on the averaged capture time. Fig.8 takes the two isotopes into account. Indeed, we see that the contribution of Ar36 decreases the scattering time of 4MeV neutrons by almost $100/mus$, which is what we expect after looking at the time to next scatter in Fig.6.

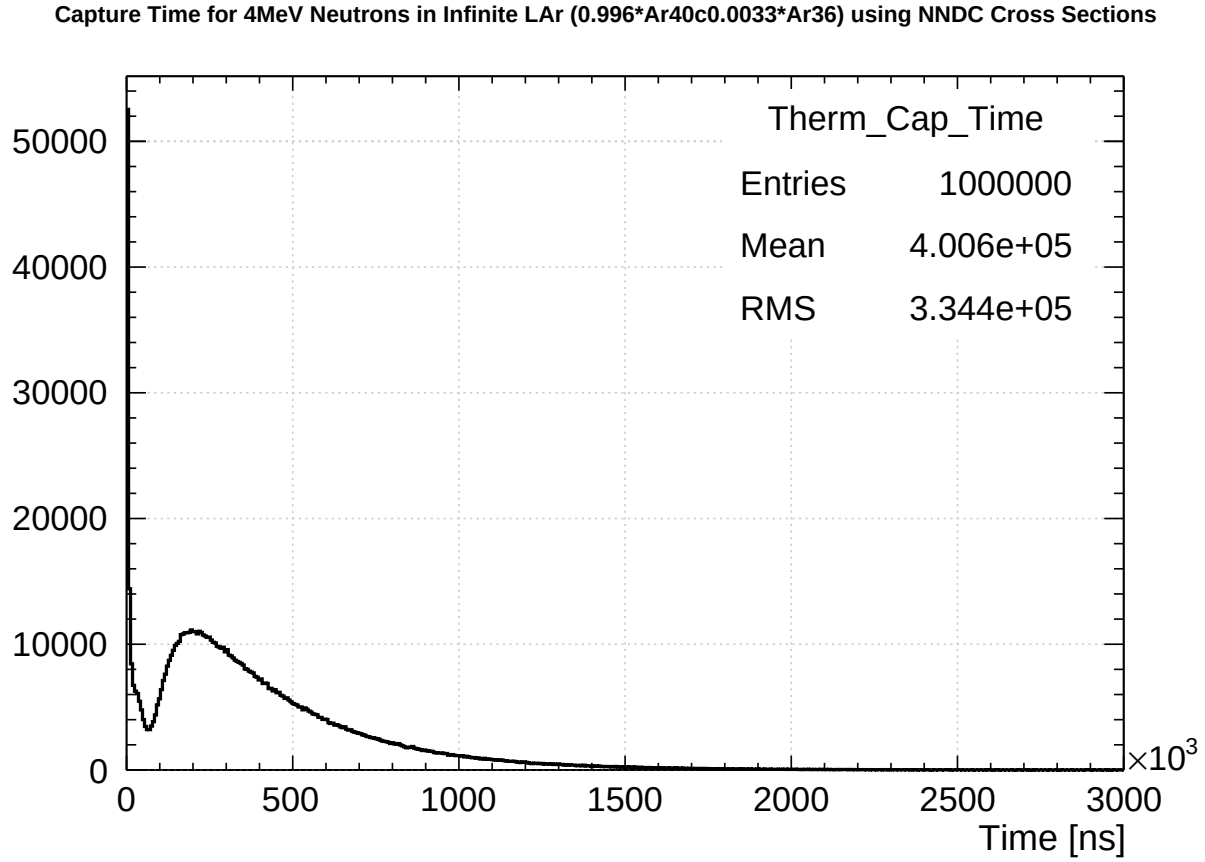

FIG.8 : Simulation of 1,000,000 neutrons in LAr, using natural abundances for Ar40 and Ar36. The shape is overall the same as in Fig.8, but the mean is shifted left.

Now the question is: how much does this matter to the ultra-pure LAr used in DEAP3600? The Q value for Ar36 captures is 8.8 Mev = 66000 PE, and Fig .... shows nothing more than a "hint" of a signal around 66k PE. As this is the summed for all of

December's neutron source runs, then it's easy to dismiss Ar36 interactions based on this data when neutron background budgets are so low as seen in Table.I .

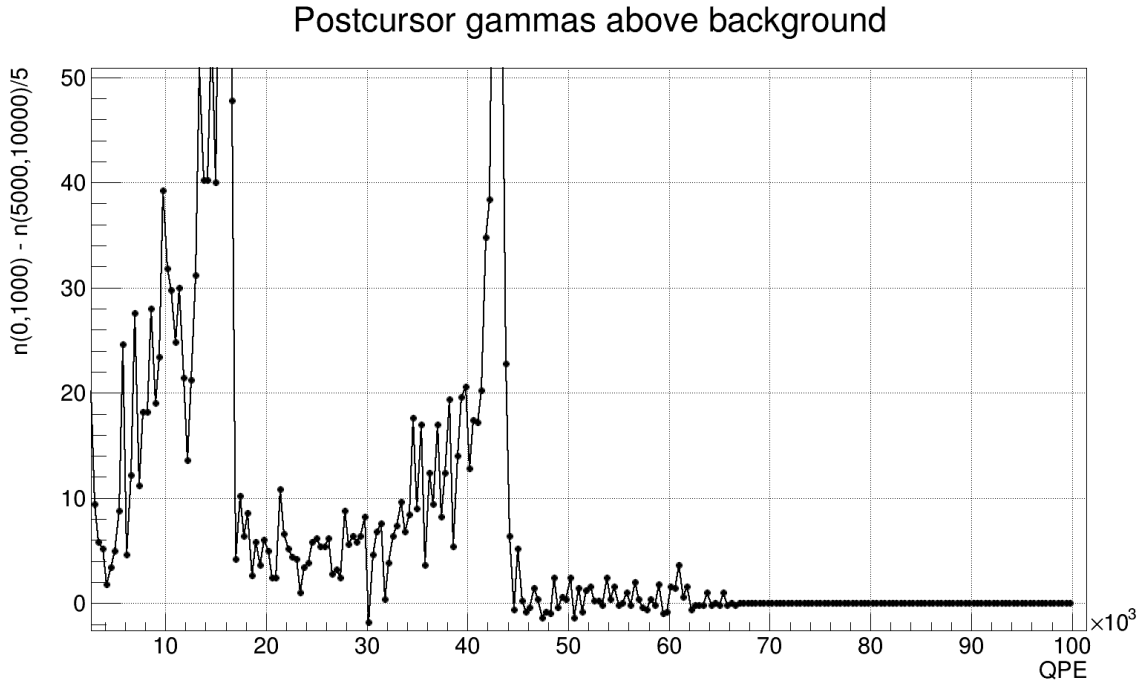

FIG.9 : Summed December neutron source-postcursor gammas. Image Credit: James Bueno 13/03/17

XI. CAPTURE TIMES IN PMMA ACRYLIC

Repeating the above analysis, but with Hydrogen-1, Cargon-12 and Oxygen-16 cross sections, and using acrylic molecules for the kinematics, $202\mu s$ is somewhat close to the $225\mu s$ vale obtained from data (Fig.13). For these elements, inelastic collisions are not a factor as H1 simply does not have an inelastic interaction, while C12 and O16 $\sigma_{inelastic}$ start around 5MeV (higher than the initial energy used here). There is also a prominent peak which results from thermalization being quickly attained by the neutrons. This is because H1 is an extremely good neutron moderator, with an energy decrement $\xi = 1$ and high σ_T. Therefore, the target thermal energy play a large part in capture times when H1 is involved. We can see that even with the addition of C12 and O16, the mean capture time is only slightly shortened.

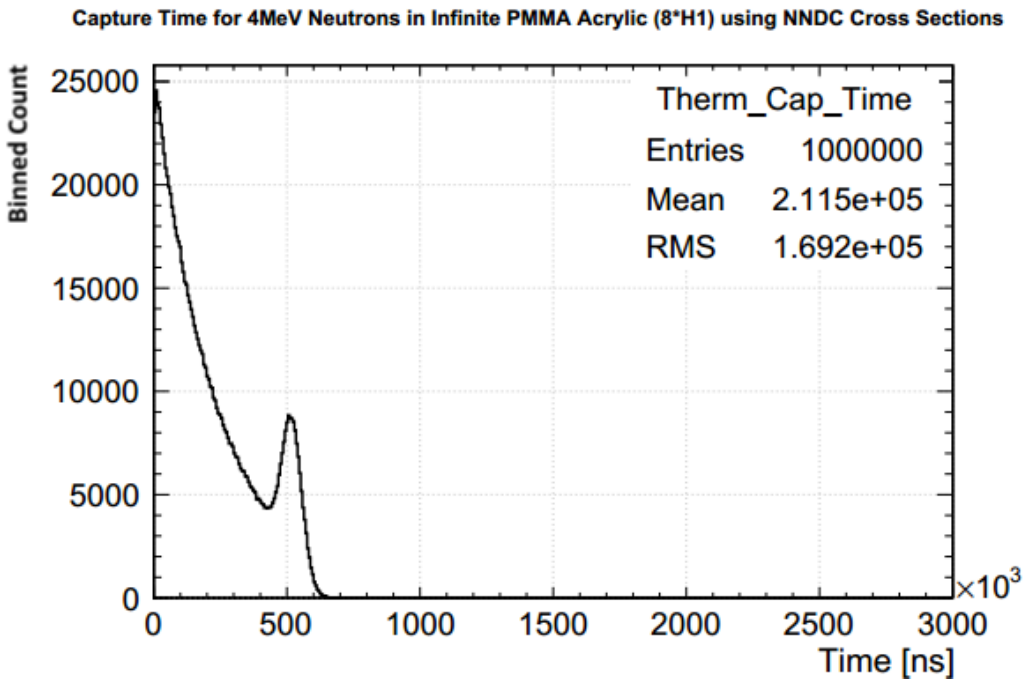

FIG.10 : Neutron captures in Acrylic, only looking at at H1 interactions.

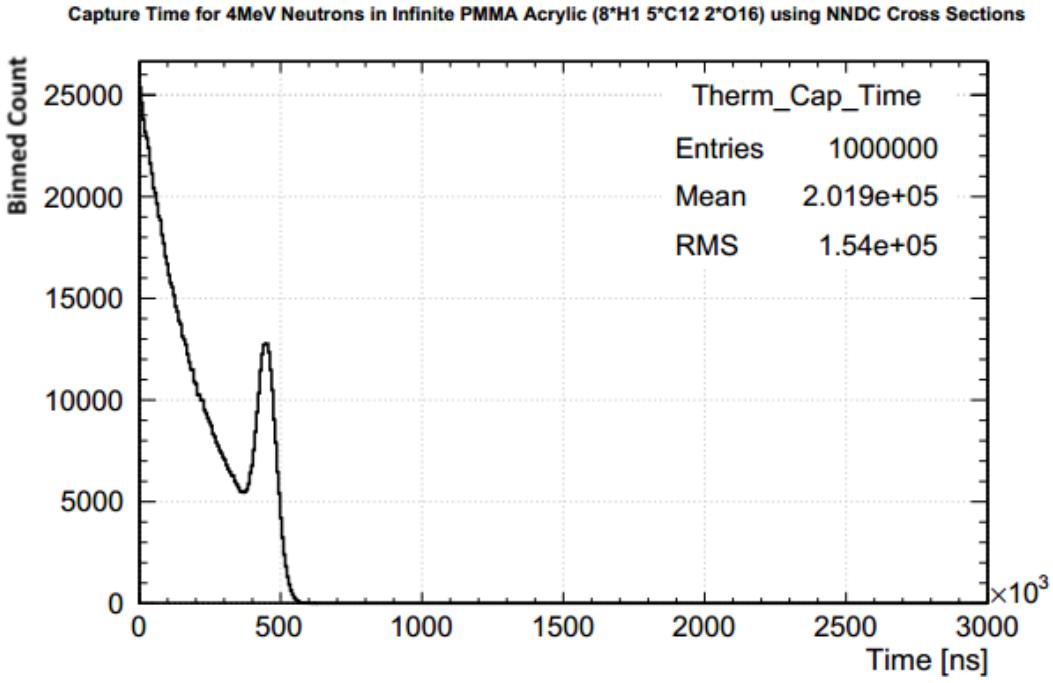

FIG.11 : Neutron captures in Acrylic, with H1, C12 and O16 accounted for. Note that this is not so different from Fig.10.

Again, we can look at gamma followers to see the actual ratio of how much the elemental components matter as measured in the detector. Fig.13 clearly shows that H1 is the prime factor, with O16 making a minor contribution. The C12 signature is essentially nonexistent.

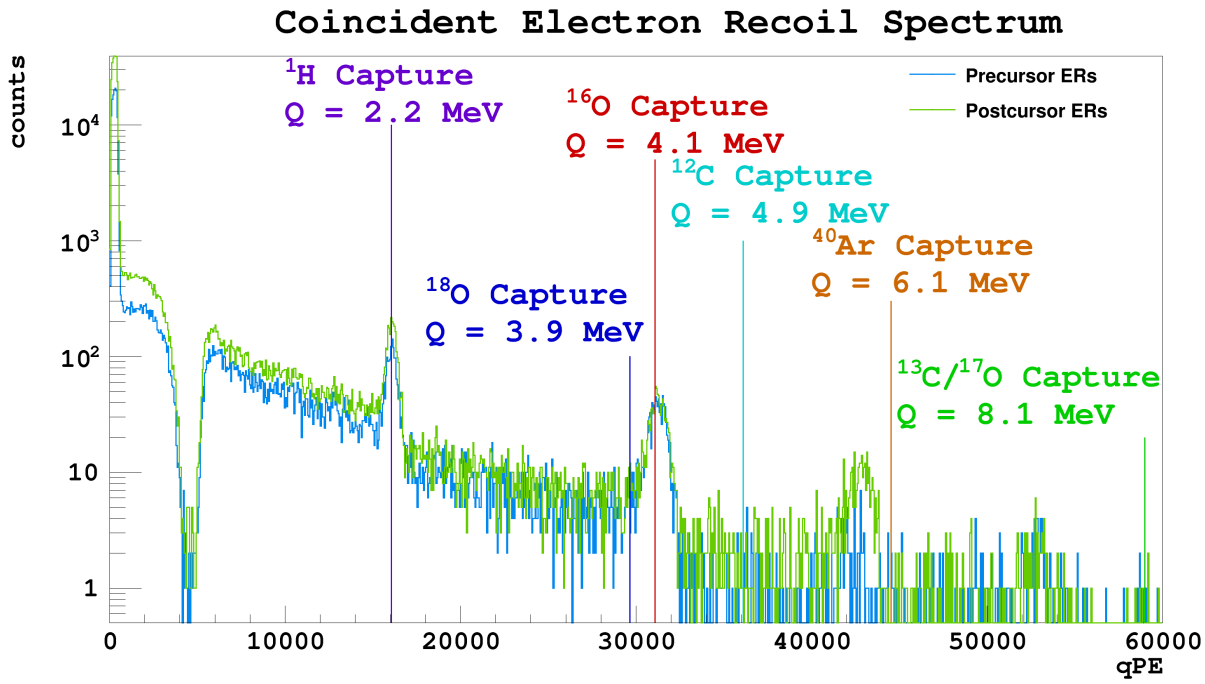

FIG.12 : Energy spectrum of electron recoils within 1 ms after the nuclear recoil or 0.5 ms before (these ranges will be more clear later). The green curve is the electron recoils that follow the nuclear recoil, while the blue curve is from electron recoils that precede the nuclear recoil. This plot labels the ER energy of the different neutron capture lines assuming a linear enery scale. Image and Caption Credit: Shawn Westerdale 03/03/17

A point to note from Shawn: "Realistically, clipping likely causes some nonlinearity, and so these lines should be moved to the left by some amount. This plot also doesn't show the lines from the AmBe gammas – notably the 4.4 MeV gamma line. The large peak around 30,000 qPE is likely due to this 4.4 MeV gamma line rather than the 16O capture, which should be comparatively rare. However, it is notable that the 40Ar capture peak seems proportionally smaller in the precursor spectrum than in the postcursor spectrum, compared to the other plots."

This plot seems to indicate that—proportionally—not too many AmBe neutrons make it through the acrylic and filler blocks. As $\sigma_T(4\text{MeV}) \approx 1.9b$ for H1, the probability of a

neutron traveling 50cm without interaction is $\exp(-50 \cdot 1.9 \cdot 1.18 \cdot 10^{-24} \cdot 6.02 \cdot 10^{23}/100) \approx 0.5$, it's unclear as to why there are so many H1 captures. It, however, is entirely possible that many neutrons scatter back into the acrylic/filler blocks and due to the high moderation (seen in Fig.14) are captured in the acrylic.

Now, looking at pure H1, as we don't know the exact thermal energy distribution, we can look at the two extremes: stopping at thermal energies and allowing the neutrons to go to absolute zero. The actual capture time will be somewhere between these two values.

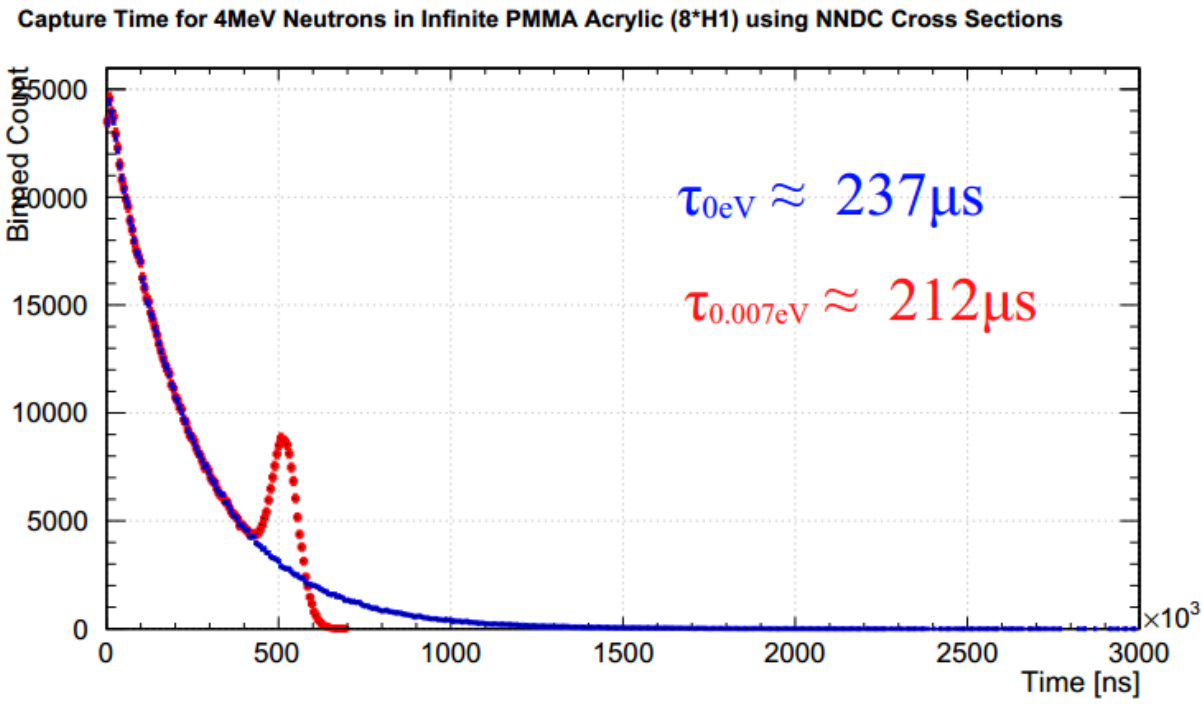

FIG.12 : Overlay of Acrylic (H1 interactions only) capture times when the acrylic is at absolute zero (blue) and when neutrons capture at thermal (red).

So we see that the capture time is somewhere between $212\mu s$ and $237\mu s$.

XII. COMPARISON OF MC TO DATA

James Bueno's data driven analysis of these results (Fig.13) gives a value of $\tau_{Ar40} \approx 492 \pm 22\mu s$[8]. This is an averaged result, and the MC gives $\tau_{Ar40} \approx 490\mu s$. These two are well within error of each other. For H1, data gives $\tau_{H1} \approx 225 \pm 7\mu s$[8], with MC giving (after averaging the two extremes) $\tau_{H1} \approx 220\mu s$, which is within error.

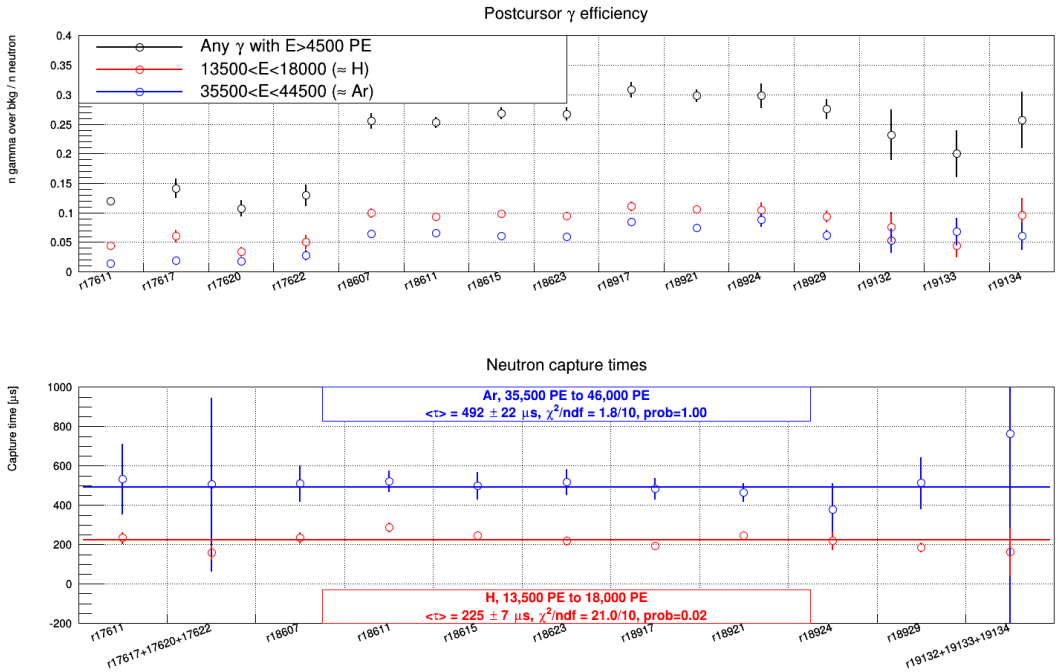

FIG.13 : Latest capture times from all neutron source runs using gamma followers in DEAP-3600 data. Image Credit: James Bueno 09/03/17

XIII. POSITION RECONSTRUCTION

WIMPs have an extremely low cross section. They therefore will only scatter once in the LAr volume, as a second scatter in a small volume has such a low probability it's not even worth thinking about. Since we use neutrons to simulate WIMPs as they both only interact via NR, it's worth asking how effective this comparison is. First, since neutrons have multiple scatters, we have to ask if the scatters sum up to be something point-like (if they were to scatter very fast and had a short mfp) or if they travel over the entire detectors diameter over a relatively long period.

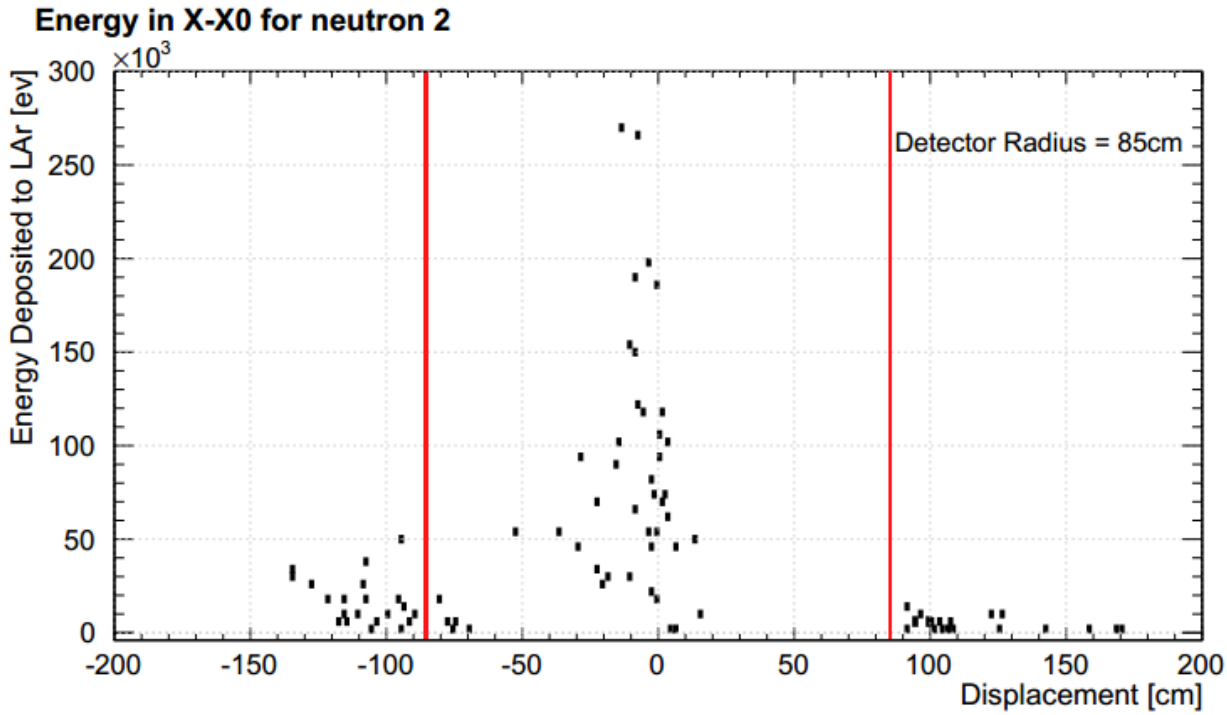

FIG.14 : The relative position (relative to x0, the first recorded interaction) of a neutron in the x-plane as it loses energy via collisions with LAr. The neutrons are generated at (0,0,0), which is the absolute ideal case in terms of space allocated for collisions. The radius of the LAr is given by the two red lines.

As seen above in Fig.14, the neutron scatters occur over the entire volume, and in fact must interact with the acrylic shell (likely filler blocks nad light guides too) even when the 4MeV neutron starts in the centre of the detector (essentially impossible in reality). From Fig.3, we can see that ten or so collisions from take, on average tens of μs, so that the overall scattering process is not very point-like.

With the addition of an acrylic shell to the MC, the ratio of capture times in LAr to PMMA can be found and compared to the ratio of electron recoils seen in Fig.12. The origin point of the neutrons can be placed outside of the acrylic shell to get a better picture of where the gamma followers on capture would most likely come from.

The addition of the acrylic shell–along with the next, Ar gas, filler blocks, light guides, PMTs, etc– was not done for this analysis, and will be included in he future as I am currently working on it.

XIV. FPROMPT ANALYSIS

A. Pulse Shape Discrimination

Since the lifetime of the singlet state is short compared to the lifetime of the triplet state, signals from nuclear recoils have a higher signal intensity at the beginning of the pulse as opposed to the EM interactions. Therefore, the PSD parameter, fractional prompt (fPrompt), is the ratio of measured light within the leading edge of the signal to the total light in the signal.

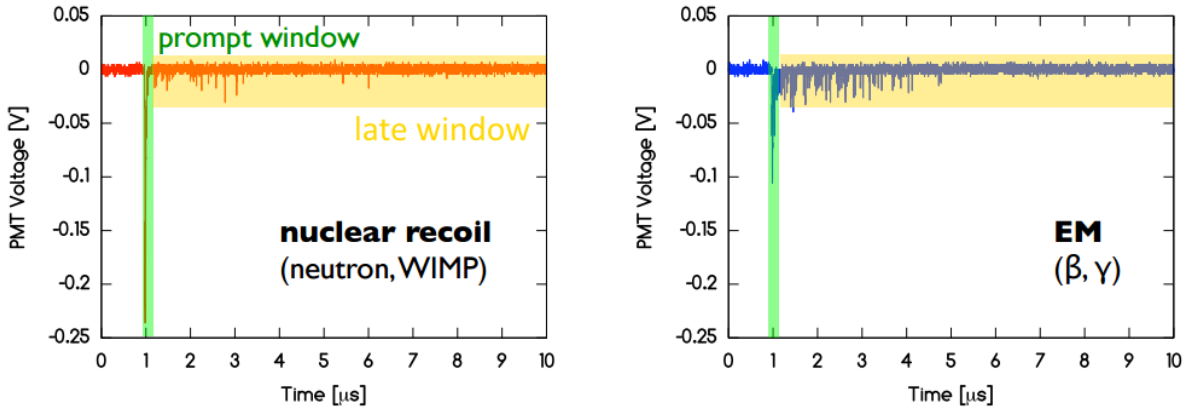

FIG.15 : Raw Waveform data taken from a PMT in DEAP-1. The shaded area is the measured light within the leading edge. This is the "prompt" window. Image Credit: Tina Pollmann 14-06-12

$$\text{fPrompt} = \frac{\text{PromptPE}}{\text{PromptPE} + \text{LatePE}} \tag{21}$$

where PromptPE is the integral of the pulse shape from t-28ns to t+Xns, with t being the leading edge of the pulse and X being the variable prompt end. The default value in DEAP-3600 is 150ns. LatePE is the integral of the pulse shape from t+Xns to t+Yns, where Y is the variable late end (around 5000ns)

By looking at multiple events over a long period of time, the amount of energy measured by the PMT for an event and the associated fPrompt can be plotted to directly show the PSD. The lifetime of the singlet light is $\tau_1 \approx 5ns$, while the lifetime of the triplet light is $\tau_3 \approx 1500ns$. Therefore, EM interactions have a low fPrompt (≈ 0.3) and nuclear recoils have a high fPrompt(≈ 0.8).

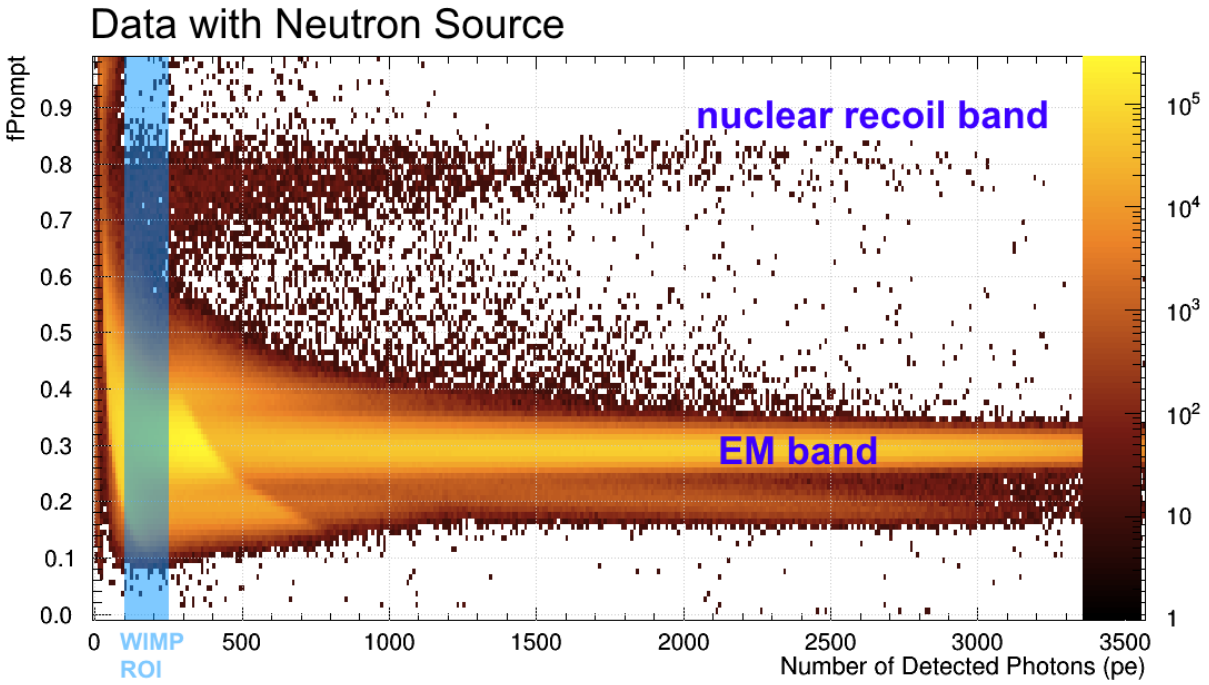

FIG.16 : Data taken from an AmBe source (neutron emitter) that illustrates the pulse shape discrimination. Here, the prompt window has a 150ns length, the current default in DEAP-3600.

Since the detector can not be completely isolated from background events, there needs to be further discrimination between recoils and background events. β particles produced from the decay of ^{39}Ar, and γ radiation dominate the background. These can be easily distinguished via PSD. α particles can not be distinguished via PSD, but they deposit an immense amount of energy that makes their signal obvious.

Recently, it has been determined that shortening the prompt window length to around 60ns (possibly down to 40ns), so a study on the fPrompt distributions of neutrons in the LAr (for natural abundances of Ar40 and Ar36) should be done. This will tell us how much of an effect the natural abundances have on the FWHM of the fPrompt Hinkley function based NR and EM bands.

B. fPrompt analysis via MC

The method of calculating fPrompt here does not take into account t0 or the scintillation response, both which could possibly flatten out the distributions. The calculation for

fPrompt shown below in Fig.17 is

$$\text{fPrompt} = \frac{\text{Energy Deposited in Prompt Window}}{\text{Energy Deposited in Long Window}}, \tag{22}$$

with a prompt window length of 60ns, and a long window length of 5000ns. This is calculated for each individual neutron.

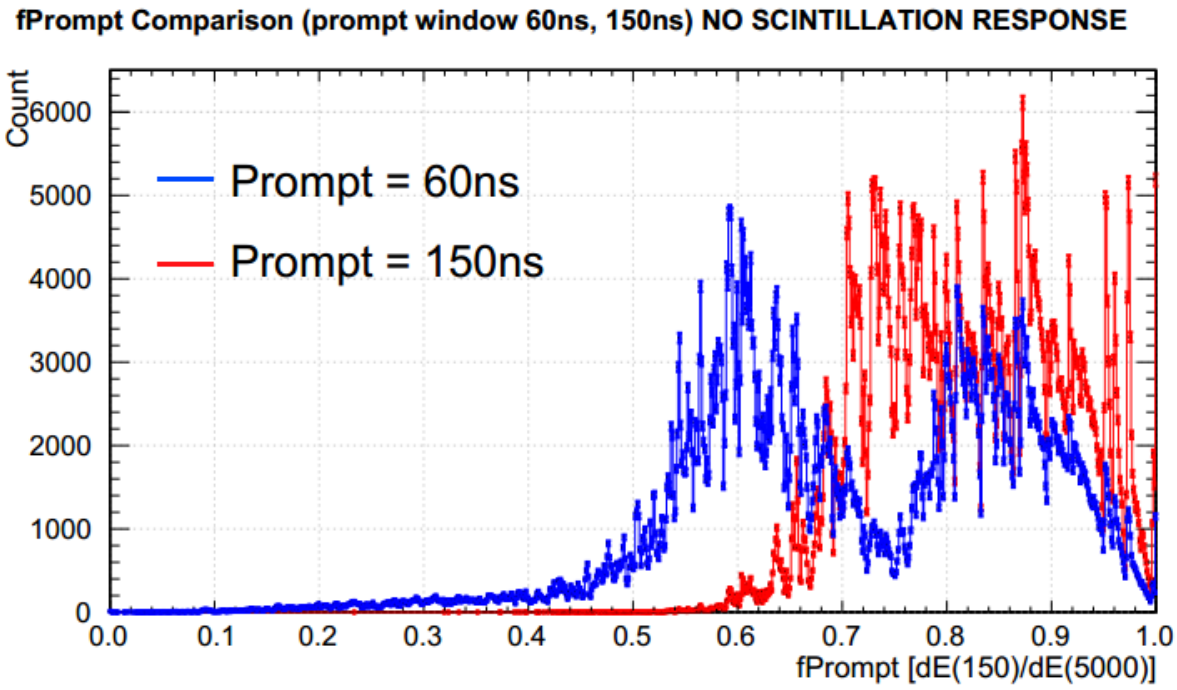

FIG.17 : fPrompt comparison between two prompt windows, 60ns (blue) and 150ns (red). Note that there are fPrompt=1 counts for the 150ns window, and nearly 0 for the 60ns window. The mean of the 60ns window ≈ 0.71, with the mean of 150ns ≈ 0.82

Right away, we see a huge difference between the two prompt lengths. This is explained in subsection "C. Energy Deposition Analysis". Essentially, the 60ns prompt ends right in the middle of the "inelastic zone", where neutrons are still scattering elastically and inelastically.

It appears that a 60ns prompt length could potentially increase the WIMP exclusion to be much higher than it currently is, but t0 and the scintillation response need to be accounted for first. There are also some fPrompt = 1.0 events with the 150ns prompt curve. This could be dangerous as if this could occur in the ROI, then there may not be a away to distinguish between a neutron and a WIMP. However, as this simulation was done with 4MeV neutrons, there could be telling signs when looking at qPE, and lower energy neutrons

would not be in the inelastic zone, and could possibly be below resonance after moderation. Further analysis is clearly needed here.

"I imagine many of the inelastic scatters will sort of veto themselves by producing a 1.4 MeV gamma, though there is probably a decent chance that the gamma is lost, and so maybe this could add a time help us with that. The RHUL group has done some simulations which they compared to AmBe data, where they were able to reproduce the AmBe neutron fprompt distribution, and then they used that to do a simulation of neutron single scatter events only, and found a bit of an increase in fPrompt. So this is possibly related."[5]

C. Energy Deposition Analysis

So to explain some of the interesting features in Figs....., we have to look at how the energy is being deposited for a large number of neutrons. Peculiarities should show themselves with the high statistics, and cross sectional features that dominate will become apparent. We can also look at Fig.3, which is a long time-scale energy deposition for a single neutron and Fig.2a, the cross sections to get an idea of some of the features.

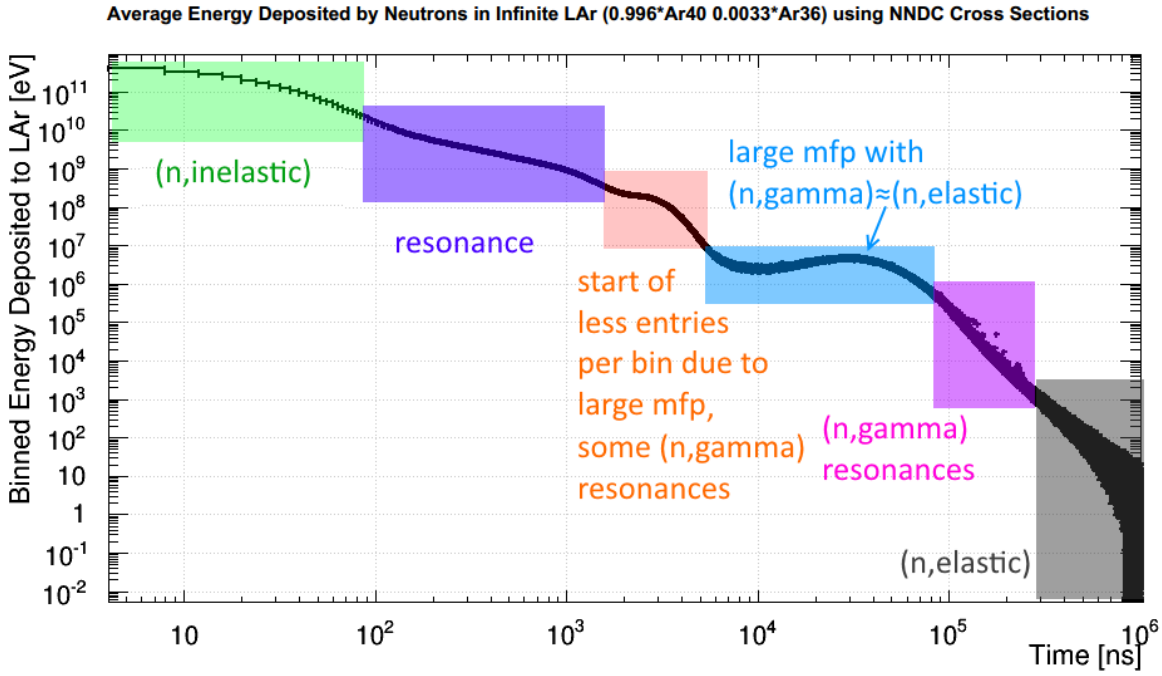

FIG.18 : Distribution of energies the neutrons (1 million) give to LAr as they collide. The dominant—or uniquely identifying—process is named for each section.

At around 100ns, the neutrons have all either been absorbed or scatter, and the inelastic interaction takes a lot more energy from the neutrons than the elastic does, causing a huge increase in deposition energy. Therefore, in Fig.18, the ~ 0.6 peak is from the neutrons that have only scattered, and the ~ 0.85 peak is from those who have been absorbed and re-emitted.

Fig.3 tells us that the extremely large mfp occurs around 10^4ns, so the flattening occurs from this large mfp. Note that the mfp is distributed around an exponential in the MC, so a flattening happening before 10^4ns makes sense.

The increase in deposited energy occuring around $5 \cdot 10^4$ns arises from $\sigma_\gamma \approx \sigma_{\text{elastic}}$, which is illustrated in Fig.18, along with two (n,γ) resonances, which get binned together with the $\sim$55keV captures, seen in Fig.2.

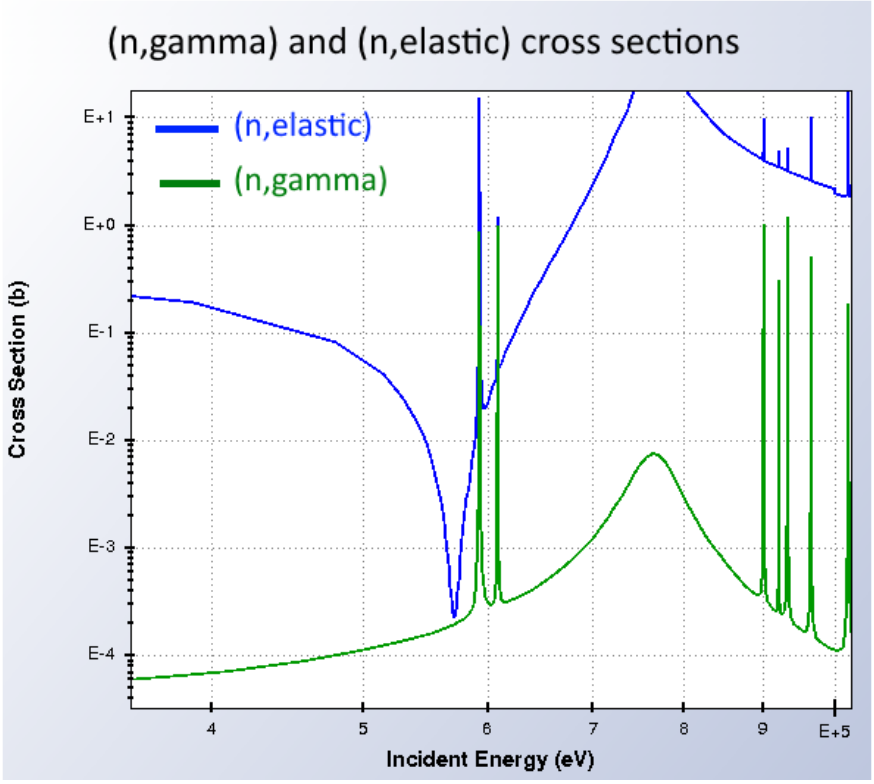

FIG.18 : Elastic and capture cross sections zoomed in on the 55keV range. Note that at the bottom of the "large mfp well", $\sigma_\gamma \approx \sigma_{\text{elastic}}$. Image Credit: NNDC, ENDF/B-VII.1 library. Retrieved March 30, 2017.

There are also a small handful of large energy deposits after the large mfp zone, which can be attributed to two (n,γ) and (n,elastic) resonances that overlap.

XV. OUTLOOK

Several additions need to be made to the MC before some results can be quotable:

- conversion to waveforms
- conversion to PE (can directly get # of expected n in ROI)
- acrylic shell addition
- t0 gaussian smearing
- convolution with scintillation response (singlet/triplet,TPB,LG)
- replication of MBlikelihood position reconstruction
- comparison to Shawn's "minimum mfp" approach for branching ratios
- light guide and filler block geometry
- neutron generation outside of volume
- 2.2MeV neutron generation in acrylic near PMT (α+C13)

XVI. CONCLUSION

The detection efficiency of neutons in DEAP-3600 is good, as the monte carlo simulation of capture times (mean 490μs) is only 0.4% off from the data obtained value (mean 492 $\pm$ 22μs). There is some ambiguity about Acrylic capture times, as the MC value (212 to 237μs) can currently only give a range of values as the thermal energy neutrons are not well simulated. The Acrylic capture times calculated from data is $225 \pm 7\mu s$. This is not an issue for LAr capture times, as less than 0.5% make it to thermal energies and therefore do not contribute much to the mean capture time.

Ar36, albeit having a significant effect on the total mean free path even when accounting for natural abundances and therefore lowering the MC mean capture time to 400μs, does not show up in a statistically significant way in the data.

Neutrons, with an MeV energy range, that make it into the LAr must interact with the acrylic vessel. This is due to the total scattering length, even when MeV neutrons are placed

at the centre of the detector, eventually placing the neutron outside the radius of the fiducial volume. The mfp also grows to several orders of magnitude greater than the diameter of the detector around 55keV.

A prompt window of 60ns could potentially increase the WIMP exclusion by a significant factor. After 60ns, half of the neutrons have not undergone the inelastic interaction, so not as much prompt light has been made. This pushes the neutron fPrompt down, away from the WIMP fPrompt.

XVII. APPENDIX

A. MC Code (bare bones)

Skipping over things like interpolating all of the NNDC data, generating TGraphs, initializing and defining variables, etc., I have included the bare minimum needed to reproduce my simulation. The full code is available upon request.

```
// read .dat and interpolate
std::ifstream inputFile("argon_total.dat");
std::string line;
std::vector<double> xt, yt;
TGraph *intergraph_total_40 = new TGraph();
int n=0;
while(getline(inputFile, line)) {
        if (!line.length() || line[0] == '#') continue;

        double c = 0., d = 0.;
        sscanf(line.c_str(), "%lf,%lf", &c, &d);
        xt.push_back(c);
        yt.push_back(d);
        intergraph_total_40->SetPoint(n++,c,d);
}

// begin simulation
for (int i = 0; i  < 1000000; ++i) {

energy = 4.0E6;
energy0 = 4.0E6;

        while (energy > 0.007) {
```

```
24
25          // angle of collision
26          angle = tr.Uniform(-1.0,1.0);
27
28          // ar40 total mfp
29          mfp_40 = tr.Exp(1. / (((intergraph_total_40->Eval(energy) * 1 * 1.4 * 1.0 * 1E↩
                -24) * 6.02E23) / 40.0));
30
31          // calcualte mfp
32          mfp_ar40e = 1. / (((intergraph_elastic_40->Eval(energy) * 1 * 1.4 * 1.0 * 1E-24) ↩
                * 6.02E23) / 40.0);
33          mfp_ar40i = 1. / (((intergraph_inelastic_40->Eval(energy) * 1 * 1.4 * 1.0 * 1E↩
                -24) * 6.02E23) / 40.0);
34          mfp_ar40g =  1. / (((intergraph_gamma_40->Eval(energy) * 1 * 1.4 * 1.0 * 1E-24) *↩
                 6.02E23) / 40.0);
35
36
37          // randomizes mfp for comparison
38          ar40e = 1. / mfp_ar40e;
39          if (energy > 41. * 1.4E6 / 40.) {
40                  ar40i = 1 / mfp_ar40i;
41                  }
42          else{
43                  ar40i = 0.;
44                  }
45          ar40g = 1. / mfp_ar40g;
46
47          \\ weight the mfps according to the total
48          sum = ar40e + ar40i + ar40g;
49          ar40e /= sum;
50          ar40i /= sum; ar40i += ar40e;
51          ar40g /= sum; ar40g += ar40i;
52
53          // determination of which interaction occurs and their kinematics
54          vel = 30.0 * sqrt(2.0 * energy / 939.0E6);
55
56          check = tr.Uniform(0.0,1.0);
57
58          if (check < ar40e) {
59                  energy = energy * (1601.0 + 80. * angle) / (41.0 * 41.0);
60                  time = time + mfp_40 / vel;
61          }
62          else if (check < ar40i) {
63                  energy = energy * (1601. * (1. - (41. * 1.4E6) / (40. * energy)) + 80. * ↩
                        angle * sqrt(1. - (41. * 1.4E6) / (40. * energy))) / (41. * 41.);
64                  time = time + mfp_40 / vel;
```

```
65          }
66          else {
67                  energy = 0.;
68                  time = time + mfp_40 / vel; // can set (n,gamma) time=NULL to filter
69          }
70
71          // change in energy after collision, and re-initialize
72          delta_energy = energy0 - energy;
73          energy0 = energy;
74
75          } // while
76
77  if (time != NULL) {
78          Therm_Cap_Time->Fill(time);
79          }
80
81  } // for
```

---

[1] Planck 2013 results. *I. Overview of products and scientific results* A&A Volume 571, (2014)

[2] Zwicky, F. *Die Rotverschiebung von extragalaktischen Nebeln*, Helvetica Physica Acta, 6: 110127, (1933)

[3] M.G. Boulay, A. Hime, *Technique for Direct Detection of Weakly Interacting Massive Particles Using Scintillation Time Discrimination in Liquid Argon* Astroparticle Physics 25 179-182 (2006).

[4] T. Heindl et al., *The scintillation of liquid Argon*, EPL 91 (2010), 62002.

[5] S. Westerdale. slack message. 5 March 2017

[6] R.A Schrack, C.D Bowman *Nuclear Cross Sections and Technology: Proceedings of a Conference, Washington, D.C., March 3-7, 1975, Volumes 1-2* U.S. Department of Commerce, National Bureau of Standards, (1975)

[7] S. Westerdale. *Analysis Note 202 Neutron Captures in AmBe Data.* https://www.snolab.ca/deap/private/TWiki/bin/view/DEAP3/AnalysisNotex202

[8] J. Bueno. *Analysis Notes 183 Events following neutrons* https://www.snolab.ca/deap/private/TWiki/bin/view/DEAP3/AnalysisNotex183

[9] V.F. Sears *Electromagnetic neutron-atom interactions.* Physics Reports Volume 141, Issue 5, Pages 281-317 (1986)

[10] F. Fernandez-Alonso, D.L. Price. *Neutron Scattering Fundamentals*, Experimental Methods in the Physical Sciences Volume 44, Pages 2-545 (2013)